ResearchGate

See discussions, stats, and author profiles for this publication at: https://www.researchgate.net/publication/5451213

Establishing Effective Simulation Protocols for β- and α/β-Peptides. II. Molecular Mechanical (MM) Model for a Cyclic β-Residue

ARTICLE *in* THE JOURNAL OF PHYSICAL CHEMISTRY B · JUNE 2008

Impact Factor: 3.3 · DOI: 10.1021/jp077601y · Source: PubMed

CITATIONS
20

READS
24

5 AUTHORS, INCLUDING:

Xiao Zhu
China University of Petroleum
35 PUBLICATIONS **765** CITATIONS
SEE PROFILE

Peter H. Koenig
Procter & Gamble
27 PUBLICATIONS **746** CITATIONS
SEE PROFILE

Qiang Cui
University of Wisconsin–Madison
201 PUBLICATIONS **13,488** CITATIONS
SEE PROFILE

Available from: Qiang Cui
Retrieved on: 25 January 2016

Establishing Effective Simulation Protocols for β- and α/β-Peptides. II. Molecular Mechanical (MM) Model for a Cyclic β-Residue

Xiao Zhu,[†] Peter Koenig,[‡] Samuel H. Gellman,[†] Arun Yethiraj,*[,†] and Qiang Cui*[,†,‡]

Department of Chemistry and Theoretical Chemistry Institute, The BACTER Institute, University of Wisconsin, Madison, 1101 University Avenue, Madison, Wiconsin 53706

Received: September 21, 2007; In Final Form: December 2, 2007

All-atom molecular mechanical (MM) force field parameters are developed for a cyclic β-amino acid, amino-cyclo-pentane-carboxylic acid (ACPC), using a multi-objective evolutionary algorithm. The MM model is benchmarked using several short, ACPC-containing α/β-peptides in water and methanol with SCC-DFTB (self consistent charge-density functional tight binding)/MM simulations as the reference. Satisfactory agreements are found between the MM and SCC-DFTB/MM results regarding the distribution of key dihedral angles for the tetra-α/β-peptide in water. For the octa-α/β-peptide in methanol, the MM and SCC-DFTB/MM simulations predict the 11- and 14/15-helical form as the more stable conformation, respectively; however, the two helical forms are very close in energy (2−4 kcal/mol) at both theoretical levels, which is also the conclusion from recent NMR experiments. As the first application, the MM model is applied to an α/β-pentadeca-peptide in water with both explicit and implicit solvent models. The stability of the peptide is sensitive to the starting configuration in the explicit solvent simulations due to their limited length (∼10−40 ns). Multiple (∼20 × 20 ns) implicit solvent simulations consistently show that the 14/15-helix is the predominant conformation of this peptide, although substantially different conformations are also accessible. The calculated nuclear Overhauser effect (NOE) values averaged over different trajectories are consistent with experimental data, which emphasizes the importance of considering conformational heterogeneity in such comparisons for highly dynamical peptides.

1. Introduction

Non-natural peptides, such as β- and α/β-peptides (oligomers of β- or of α- and β-amino acid residues, respectively), have attracted interest in recent years due to their potential in biomedical and materials applications.[1,2] However, due to the limited amount of quantitative structural and dynamical information, the sequence−structure−property relationships in these systems are not well understood.[3−14] For example, β[3]-residues that bear a sidechain branch point adjacent to the backbone, such as β[3]-hVal, have been suggested to promote helix formation,[15,16] but this idea has been challenged.[17]

Molecular simulations are becoming increasingly useful in the study of biomolecular systems,[18,19] and simulations can provide detailed energetic and dynamic information for complex biomolecules, which allow us to address mechanistic questions of interest at an atomic scale. The simulation results, of course, are usually sensitive to the molecular force field used for the intramolecular and intermolecular interactions.[20] For example, Hu et al.[21] have shown that the predictions for the ϕ/ψ distributions of dihedral angles in di-alanine and di-glycine in solution are *qualitatively* different in various force fields such as CHARMM22,[22] GROMOS,[23] AMBER,[24] and OPLS.[25]

For natural proteins and nucleic acids, several molecular force fields have been developed and carefully tested.[23−26] For non-natural peptides, however, most previous simulation studies simply "borrow" parameters from existing force fields without systematic benchmark studies.[27−35] Therefore, although the qualitative features revealed in those studies are valuable, the quantitative accuracy of the results remains uncertain.

The long-term goal of our research is to develop a "bottom-up" approach for simulating β- and α/β-peptides that starts from atomic-level models and systematically propagates to larger and coarser length scales.[36] In this way, the connection between the sequence, structure, and material properties of these non-natural peptides can be systematically analyzed. To facilitate the development of atomic-level molecular force fields for the β- and α/β-peptides, we take a hierarchical protocol in which the hybrid quantum mechanical/classical mechanical (QM/MM)[37−40] simulations are used as the reference. In particular, the SCC-DFTB approach[41,42] is used to describe the peptide, and MM models are used to describe the solvent (water or methanol).[43] In our recent work,[36] we have carefully benchmarked the SCC-DFTB approach for several β- and α/β-peptides in both the gas phase and solution against high-level ab initio calculations and available experimental data. The results support the use of the SCC-DFTB/MM simulations as a uniquely meaningful reference for the development of MM models for these systems, which typically lack highly quantitative experimental structural information.

In this work, as the first example, we develop MM parameters for peptides that contain *trans*-2-amino-cyclo-pentane-carboxylic acid (ACPC), a conformationally constrained β-amino acid. This is of interest because ACPC has been used in the design of many β-peptides due to its ability to enhance helix formation.[4,14,44] The MM model is tested on a tetra-α/β-peptide and an octa-α/β-peptide, for which the results compare favorably to SCC-DFTB/MM simulations in terms of the distribution of key torsional angles and relative energetics of different helical forms. The MM model is then applied to a longer (15-mer) α/β-

* To whom correspondence should be addressed. E-mail: yethiraj@chem.wisc.edu (A.Y.), cui@chem.wisc.ed (Q.C.).
[†] Department of Chemistry and Theoretical Chemistry Institute.
[‡] The BACTER Institute.

10.1021/jp077601y CCC: $40.75 © 2008 American Chemical Society
Published on Web 04/11/2008

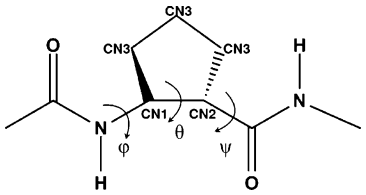

Figure 1. Structure of the parametrization model. New atom types are labeled next to each atom.

peptide with both explicit and implicit solvent models; the results are consistent with the experimental signatures for stable conformations. At the nanosecond timescale, however, the peptide exhibits significant structural fluctuations, especially in the implicit solvent simulations.

2. Methods

Our general strategy is to develop MM parameters for β-amino acid(s) in the framework of the CHARMM22 all-atom force field.[22] Provided that we follow a similar parametrization procedure, the parameters should be compatible with the CHARMM22 force field for α-amino acids, which makes it possible to study both β- and α/β-peptides with the current MM model.

The CHARMM22 all-atom force field expresses the potential energy of the system in the form,

$$U(\vec{R}) = \sum_{\text{bonds}} K_b(b - b_0)^2 + \sum_{\text{angles}} K_\theta(\theta - \theta_0)^2 + \sum_{\text{UB}} K_{\text{UB}}(S - S_0)^2 + \sum_{\text{dihedrals}} K_\chi(1 + \cos(n\chi - \delta)) + \sum_{\text{impropers}} K_{\text{imp}}(\phi - \phi_0)^2 + \sum_{\text{nonbond}} \left\{ \epsilon_{ij}\left[\left(\frac{R_{\min_{ij}}}{r_{ij}}\right)^{12} - \left(\frac{R_{\min_{ij}}}{r_{ij}}\right)^{6}\right] + \frac{q_i q_j}{\epsilon_1 r_{ij}} \right\} \quad (1)$$

where K_b, K_θ, K_{UB}, K_χ, and K_{imp} are the bond, angle, Urey−Bradley, dihedral angle, and improper dihedral angle force constant, respectively; b, θ, S, χ, and ϕ are the bond length, bond angle, Urey−Bradley 1,3-distance, dihedral angle, and improper torsional angle, respectively, with the subscript zero representing the equilibrium values for the individual terms. Coulombic and Lennard-Jones (L-J) 6−12 terms contribute to the nonbonded interactions; ϵ is the L-J well depth and $R_{\min}$ is the position of the minimum, q_i is the partial atomic charge, ϵ_1 is the effective dielectric constant, and r_{ij} is the distance between atom i and j.

For ACPC, both bonded and nonbonded parameters are developed. For the nonbonded parameters, which include ϵ and $R_{\min}$ for the L-J terms and partial charges (q_i) for the electrostatics, we assign values based on similar atom types (e.g., hybridization type) in the CHARMM22 force field since the sidechain is rather apolar. To parametrize for the bonded terms, a diamide derivative of ACPC is used (see Figure 1). Two different fitting procedures are tested. The first approach is referred to as the automated frequency matching method (AFMM),[45−47] which fits the MM parameters based on matching the vibrational frequencies and eigenvectors from QM calculations for the model compound.[47] The second fit is done using a multi-objective evolutionary algorithm (MOEA), which was developed by Mostaghim, Hoffmann, Koenig, and co-workers.[48] In this more elaborate approach, a multi-objective evolutionary algorithm with a set of physically motivated objective functions is used to optimize the MM (bonded) parameters. In particular, we focus on reproducing the geometries, vibrations, and energetics of different conformers of the compound at a QM level. To be consistent with the CHARMM22 force field, all reference calculations for both the AFMM and MOEA based fitting are done at the Hartree−Fock (HF) level with the 6-31G* basis set[49] using Gaussian03.[50]

Following the parametrization, the di-peptide derivative (the ACPC-Ala di-peptide) and a tetra-α/β-peptide (ACPC-Ala-ACPC-Ala) in aqeous solution as well as an octa-α/β-peptide (ACPC-Ala-ACPC-Ala-ACPC-Ala-ACPC-Ala) in methanol are chosen as test systems. Full MM simulations are compared to SCC-DFTB/MM simulations in which the α/β-peptide is treated using the standard parametrization of SCC-DFTB.[41]

For both the di- and tetra-α/β-peptides, the solvation occurs in an 18 water sphere, and the generalized solvent boundary potential (GSBP)[51] is used for the boundary condition with a 2 water exclusion radius.[51] Atoms in the spherical shell from 13 to 16 are treated with Langevin dynamics, and the rest are treated with Newtonian dynamics.[52] A time step of 1.0 fs is used, and all bonds to hydrogen atoms are constrained with SHAKE.[53] For the di-α/β-peptide, 24 (24) ns of MD simulations are carried out at the SCC-DFTB/MM (MM) levels; for the tetra-α/β-peptide, it is 2 (5) ns. With these equilibrium simulations, both the distributions and potentials of mean force along the key dihedral angles (ϕ,ψ,θ) are monitored.

For the octa-α/β-peptide simulation, the methanol molecules are treated using the MEOH model in the CHARMM22 all-atom force field,[22] which has been shown to describe the bulk property of methanol rather well with both periodic boundary and GSBP simulations.[36] The α/β-peptide is solvated in a 20 methanol sphere around its center of mass, with a 2.5 methanol exclusion shell associated with the GSBP setup. The system contains a total of 357 MEOH methanol molecules and 117 peptide atoms. Similar to the previous work,[36] the potential of mean force for the conversion between 14/15- and 11-helices is estimated using umbrella sampling.[54] The reaction coordinate is chosen to be the end-to-end distance between the amide nitrogen in the first residue and the carbonyl carbon in the last residue, and the sampled range is between 10.6 and 18.0 Å with 37 windows. To generate the initial structures for each window, a 14/15-helix is pulled toward the 11-helix with the approximate reaction coordinate, and intermediate structures are collected every 0.2 Å. Each window includs 25 ps of equilibration and 75 ps of production calculations. The weighted histogram analysis method (WHAM)[55] is used to obtain the PMF. To check the convergence of PMF calculations, runs with different starting structures or random seeds for velocity assignment are performed (see the Supporting Information for details).

2.1. Molecular Dynamics of Pentadeca-peptide. The pentadeca-α/β-peptide (ACPC-Lys-ACPC-Tyr-APC-Glu-APC-Leu-ACPC-Tyr-ACPC-Lys-APC-Ala-APC), where APC is aminopyrrolidine-carboxylic, has been characterized qualitatively by Schmitt et al. in aqueous solution using NOE experiments.[44] Although nonsequential backbone NOEs suggested that a 14/15-helix was the preferred conformation, the detailed structure and structural distribution are not known. Therefore, molecular dynamics simulations can complement the NOE study to provide a more concrete characterization.

Specifically, we perform both explicit and implicit solvent simulations with the developed MM parameters starting from two different initial structures: a 14/15-helix built from the NOE derived structure as reported by Schmitt et. al.[14] and an 11-helix built based on the crystal structure for a slightly different system where the α-amino acids are aminoisobutyric acid.[14] The residue APC is replaced by ACPC, which should not affect the

TABLE 1: Bond Parameters for ACPC[a]

atom types	K_b (kcal mol^{-1} Å^{-2})	b_0 (Å)	atom types	K_b (kcal mol^{-1} Å^{-2})	b_0 (Å)
C−CN2	262.0	1.533	HA−CN3	307.6	1.085
CN1−CN2	250.0	1.562	HB−CN1	325.0	1.082
CN1−CN3	215.0	1.532	HB−CN2	325.0	1.459
CN2−CN3	215.0	1.545	NH1−CN1	305.6	1.459
CN3−CN3	215.0	1.532			

[a] Only parameters not published in ref 22 are shown.

results significantly since the APC was introduced in the experiment mainly due to solubility issues.

In the explicit solvent simulation, the peptide is solvated in a rhombic dodecahedron (RHDO) water box with the TIP3P model.[56] The SHAKE[53] algorithm is used for all bonds involving hydrogen to allow a time step of 2 fs. A switching scheme[57] for interatomic distances between 10 and 12 Å is applied for van der Waals interactions and long-range electrostatics are treated with the particle-mesh Ewald method.[58] Two independent production runs on the order of 10−40 ns for each starting structure are performed under the constant temperature and pressure condition. The temperature is constrained using the Nóse−Hoover algorithm,[59,60] with a mass of 250 amu for the thermostat and a Hoover reference temperature equal to the desired system temperature (300 K). The pressure is controlled with the Anderson algorithm,[61] with a mass of 500 amu for the pressure piston, a reference pressure of 1 atm, a Langevin piston collision frequency of 10 ps^{-1}, and a Langevin piston bath temperature equal to the desired system temperature.

For the implicit solvent simulations, the generalized Born with smooth switching method (GBSW)[62] is used. This model has been shown to provide a reasonable balance between computational efficiency and accuracy.[63] We use the set of atomic radii optimized by Nina and co-workers[64] as input of the distance-independent atomic radii for the atom types available. For new atom types created in current work for the β-amino acid, regular Cα values are used for the two main-chain carbon atoms, and those for the sidechain carbon atoms are taken from proline. The hydrogen atomic radii are set to zero by convention. For the dielectric switching, a switching length of 0.4 Å is used along with 38 Lebedev angular integration points and 24 radial integration points up to 20 Å for each atom.[62] Using a "molecular surface"[65] has been found to generate stable MD trajectories,[66] and therefore, this protocol is employed here with the corresponding Born radii coefficients of $C_0 = 1.204$ (coefficient for the Coulomb field approximation term) and $C_1 = 0.187$ (coefficient for the correction term).[63] The effective Born radii are updated every other molecular dynamics step for computational efficiency. The nonpolar contribution to the solvation free energy is estimated based on the standard solvent-accessible surface area (SASA) model, and the surface tension coefficient is set to 0.003 kcal mol^{-1} Å^{-2}. To be compatible with the way that GBSW was parametrized,[62] we use 20 Å cutoff for nonbonded interactions. All GBSW simulations are carried out at 300 K using Langevin dynamics with a simple scheme in which all non-hydrogen atoms are assigned with the same friction coefficient of 25 ps^{-1}. Similar to explicit solvent simulations, the SHAKE[53] algorithm is used to constrain all bonds involving hydrogen atoms and a time step of 2 fs is used. To sample the conformational space efficiently,[67] at least 10 GSBW trajectories with different initial atomic velocities are calculated with both starting structures (14/15- and 11-helices) and each trajectory is run for 20 ns.

To analyze the results, occupancy of backbone hydrogen bonds and ensemble-averaged NOE distances are calculated for both explicit and implicit solvent simulation. The criterion for hydrogen bond formation is set as follows: the maximum distance between hydrogen bond acceptor C═O and hydrogen bond donor N−H is 2.4 Å, and the minimum angle of (C═)O···H−N is 125°. NOE distances are obtained by calculating the nonlinear average proton−proton distances, i.e., $\bar{r} = (\langle r^{-3} \rangle)^{-1/3}$, corresponding to a slowly tumbling molecule.[68]

For the implicit solvent simulations, cluster analysis is performed using the MMTSB toolkit[69] to determine the representative confomers sampled during these trajectories. Structures of the peptide are extracted from the trajectories every 10 ps, which are then grouped based on the backbone rmsd for residues 2−14 with a cutoff radius of 3 Å.

3. Results and Discussion

In this section, we first compare results for several short α/β-peptides at the MM and QM (SCC-DFTB)/MM levels to validate the MM model. Next, we present results from MM simulations for a longer α/β-peptide and discuss the findings in the context of the recent NMR study.[44]

3.1. Parametrization and Validation of the MM Model. As illustrated in Figure 1, three new atom types are created for the cyclic β-amino acid (ACE-ACPC-NMA): CN1 for the β-carbon, CN2 for the α-carbon in backbone, and CN3 for other carbon atoms in the five-membered ring. There are in total 9 bond terms, 22 angle terms, 4 Urey−Bradley terms, and 22 torsional terms. The equilibrium bond lengths and bond angles are taken from the global minimum structure at the HF/6-31G* level, to be consistent with the CHARMM22 force field.[22] All the equilibrium values and force constants parametrized using the MOEA procedure are listed in Tables 1−4. Test calculations have shown that the parameters developed with the simpler AFMM procedure are less reliable, especially in terms of the distribution along the critical θ degree of freedom (Figure 1), which emphasizes the importance of careful parametrization for quantitative results; for details, see the Supporting Information. From this point on, only the MOEA paramaterized model will be considered in the discussion of MM results.

TABLE 2: Angle Parameters for ACPC[a]

atom types	K_θ (kcal mol^{-1} rad^{-2})	θ_0 (deg)	atom types	K_θ (kcal mol^{-1} rad^{-2})	θ_0 (deg)
CN1−CN2−C	39.4	110.5	HB−CN1−CN2	27.0	111.6
CN1−CN2−CN3	62.6	105.1	HB−CN1−CN3	27.0	110.5
CN1−CN3−CN3	61.7	104.3	HB−CN1−NH1	41.2	107.6
CN1−NH1−C	104.0	122.6	HB−CN2−C	45.0	107..0
CN2−CN1−CN3	62.6	105.4	HB−CN2−CN1	27.0	109.8
CN2−CN3−CN3	61.7	104.3	H−NH1−CN1	45.4	118.4
CN2−C−NH1	106.1	114.2	NH1−CN1−CN3	64.5	110.9
CN2−C−O	97.1	122.9	NH1−CN1−CN2	64.5	111.6
CN3−CN2−C	45.4	113.1	CN3−CN3−CN3	61.7	104.3

[a] Only parameters not published in ref 22 are shown.

TABLE 3: Angle Parameters with Urey−Bradley Term for ACPC[a]

atom types	K_θ (kcal mol^{-1} rad^{-2})	θ_0 (deg)	K_{UB} (kcal mol^{-1} Å^{-2})	S_0 (Å)
HA−CN3−CN1	24.7	110.0	19.5	2.1790
HA−CN3−CN2	24.7	111.0	19.5	2.1790
HA−CN3−CN3	24.7	113.0	19.5	2.1790
HA−CN3−HA	35.0	107.4	5.7	1.8020

[a] Only parameters not published in ref 22 are shown.

3.1.1 Di-α/β-peptide (ACPC-Ala) in the Gas Phase and Water. As shown in Figure 2a and b, the distributions along the ϕ, θ, and ψ torsions are very similar at the MM and SCC-DFTB levels for the ACPC-Ala di-peptide in the gas phase. This is largely expected because the MM parameters are developed using the same molecule, although only discrete quantities (e.g., relative energetics of different conformers) are explicitly used in the fitting procedure; further correcting the torsional profiles in a continuous fashion as done in the CMAP approach[70] is difficult due to the higher (3) backbone-torsional dimension for β-amino acids. It is encouraging to see (Figure 2c and d) that the distributions in water are similar at the MM and SCC-DFTB/MM levels, especially concerning the position of peak distributions. The only notable difference occurs in regions with large ϕ (approx −120 to −150°) and θ (approx −60°) values, for which the MM model (Figure 2c) gives larger amplitudes and a narrower distribution in θ (also see the Supporting Information).

3.1.2 Tetra-α/β-peptide (ACPC-Ala-ACPC-Ala) in Water. For the tetra-α/β-peptide in solution, the distributions along the ϕ, θ, and ψ torsions at the MM and SCC-DFTB/MM levels follow a trend similar to that seen in the di-peptide case although smaller regions are sampled in the shorter tetra-peptide simulations (see Supporting Information Figures S1−S4 for detailed plots). For example, at the SCC-DFTB/MM level, the α/β-peptide is flexible during the 2 ns of simulation; in particular, a wide range of θ values is sampled with a weak bimodal distribution. With the MM model, the θ distribution is largely consistent with the SCC-DFTB/MM result with a similar breadth although the MM distribution is less uniform and exhibits three small peaks (Figure S1). Correspondingly, the θ-PMF minimum at the SCC-DFTB/MM level is around $\theta \sim 140°$. At the MM level, however, the PMF is more structured and the deepest minimum is at $\theta \sim 70°$. Nevertheless, the difference between the SCC-DFTB/MM and MM results is usually smaller than 2 kcal/mol.

The distributions in ϕ and ψ agree less well between the MM and SCC-DFTB/MM simulations (Figure S1 in the Supporting Information). For ϕ, the MM peak distribution shifts by $\sim 50°$ from the SCC-DFTB/MM result; for ψ, almost the entire region is sampled with SCC-DFTB/MM while the MM model rarely samples the regions (−50°, 50°). Overall, however, the performance of the MM model is quite acceptable especially concerning the projection involving the key θ degree of freedom (i.e., $\theta - \phi$ and $\theta - \psi$ maps; see Figures S2−S4).

3.1.3 Octa-α/β-peptide (ACPC-Ala-ACPC-Ala-ACPC-Ala-ACPC-Ala) in Methanol. For the octa-α/β-peptide in methanol, the NOE data set for the closely related sequence (ACPC-Lys-APC-Tyr-ACPC-Glu-APC-Ala) suggest that both 14/15- and 11-helices are present.[13] At the SCC-DFTB/MM level,[36] the PMF result is consistent with this suggestion and finds that the 11-helix is slightly more stable than the 14/15-helix by a few kilocalories per mole. With the current MM model, the two helical forms are also rather close in free energy although the 14/15-helix is now more stable by ∼2 kcal/mol (Figure 3a). The backbone hydrogen bond occupancy (Figure 3b) suggests that both helical forms are equally populated.

Although opposite trends for the relative stability of the 14/15- and 11-helices are found at the SCC-DFTB/MM and MM levels, it is useful to note that the SCC-DFTB approach was found in our previous benchmark calculations[36] to underestimate the stability of the 14/15-helix. Therefore, considering that the energetic biases are small at both levels, it is likely that the characteristics observed with the current MM model are realistic.

3.2. Molecular Dynamics of Pentadeca-α/β-peptide. *3.2.1. Explicit Solvent Simulations.* With the 14/15-helix as the starting structure, the α/β-peptide has a dynamical structure but overall remains close to the 14/15-form. In particular, the backbone rmsd is smaller than 2 Å from the starting structure in the first nanosecond. Then, the N-terminus starts to deviate from the ideal 14/15-conformation while the rest of the helical structure is well-maintained within 3 ns as indicated by the backbone rmsd for residues 4−11 (Figure 4a). Next, the helical structure close to the N-terminus continues to melt and the rmsd increases to more than 3 Å even when only residues 4−11 are considered; for a snapshot, see Figure 5b. Remarkably, in one of the two trajectories (Figure S6 in the Supporting Information) the 14/15-helical structure recovers after another 4 ns and the rmsd value reduces back to around 2 Å. The occupancies of characteristic $i,i+4$ backbone hydrogen bonds are very high, and these hydrogen bonds exist for at least half of the simulation time (Figures 4b and S6b). In other words, the 14/15-helical structure is overall rather stable for at least the central part of the helix during the majority of the explicit solvent simulations, although rather different conformations are sampled during this time. Such structural heterogeneity has been commonly found in other simulations of natural[71] and non-natural peptides.[29,72−75]

The conformational heterogeneity should have a substantial impact on the ensemble properties such as NOE. In Table 5,

TABLE 4: Dihedral Parameters for ACPC[a]

atom types	K_χ (kcal mol^{-1})	N	χ_0 (deg)	atom types	K_χ (kcal mol^{-1})	N	χ_0 (deg)
CN1−NH1−C−O	0.2	2	180.0	H−NH1−CN1−CN3	−0.2	1	0.0
CN1−NH1−C−CT3	1.2	1	0.0	HB−CN1−NH1−C	0.5	1	0.0
CN1−NH1−C−CT3	2.2	2	180.0	HB−CN1−NH1−H	−0.4	1	0.0
CN2−C−NH1−CT3	1.2	1	0.0	X−CN1−CN2−X	0.1	1	0.0
CN2−C−NH1−CT3	1.6	2	180.0	X−CN1−CN2−X	−0.2	2	0.0
CN2−CN1−NH1−C	1.3	2	180.0	X−CN1−CN2−X	0.2	3	0.0
CN2−CN1−NH1−C	0.6	4	0.0	X−CN1−CN3−X	0.1	3	0.0
CN2−C−NH1−H	2.1	2	180.0	X−CN2−CN3−X	0.2	3	0.0
CN3−CN1−NH1−C	1.5	2	180.0	X−CN2−C−X	0.3	1	0.0
CN3−CN1−NH1−C	0.2	4	0.0	X−CN2−C−X	0.4	2	0.0
H−NH1−CN1−CN2	0.4	1	0.0	X−CN3−CN3−X	0.1	3	0.0

[a] Only parameters not published in ref 22 are shown.

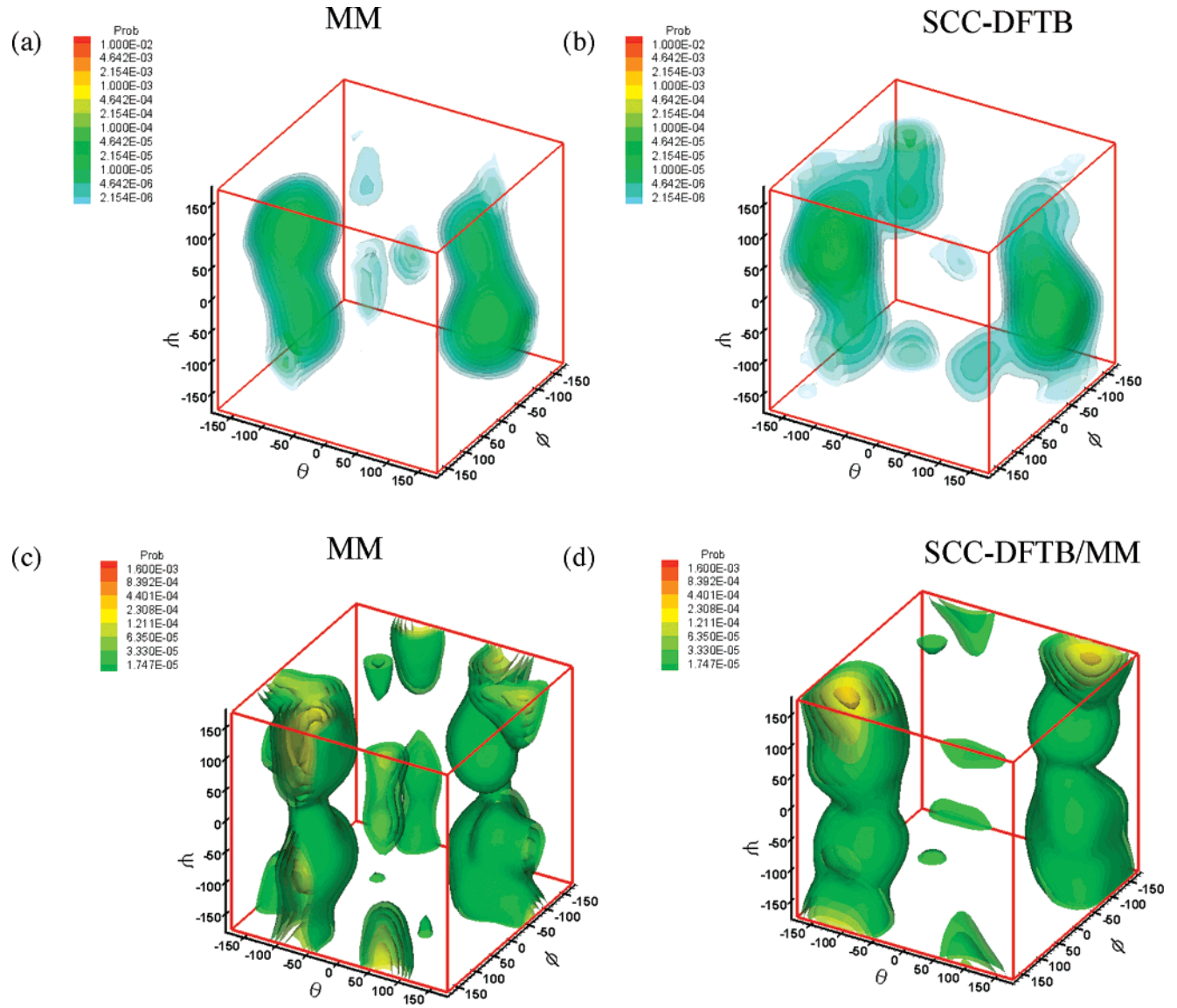

Figure 2. Comparison of distributions of key torsional angles (ϕ, θ, and ψ) from SCC-DFTB/MM (24 ns) and full MM simulations (24 ns) for a di-α/β-peptide (ACPC-Ala) in the (a and b) gas phase and (c and d) water.

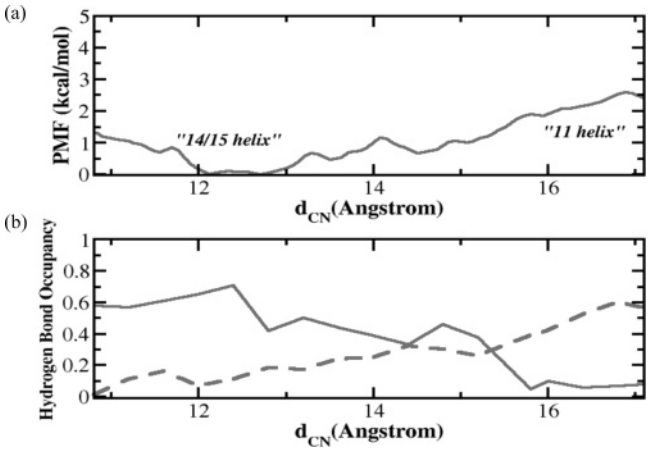

Figure 3. Results from MM simulations for an octa-α/β-peptide (ACPC-Ala-ACPC-Ala-ACPC-Ala-ACPC-Ala) in methanol solution. (a) PMF for the conversion between the 14/15-helix and 11-helix. (b) Hydrogen-bonding occupancy analysis (solid line 14/15-helix; dashed line 11-helix).

we compare the experimental nonsequential backbone NOE data to the average proton−proton distances calculated from the simulations. In most cases, attention has been paid mainly to "positive violations", where computed average distances from simulations are greater than the NOE derived upper-bound distance values. Such positive violations in explicit solvent simulations occur only for the pairs $2_\alpha H_\alpha \rightarrow 5_\beta H_\alpha$, $1_\beta H_\beta \rightarrow 5_\beta HN$, $1_\beta H_\beta \rightarrow 4_\alpha HN$, $3_\beta H_\beta \rightarrow 6_\alpha HN$, $10_\alpha H_\alpha \rightarrow 13_\beta H_\alpha$, and $12_\alpha H_\alpha \rightarrow 15_\beta H_\alpha$, and all violations are within 1.0 Å. Three of these NOEs involve the first or last residue, which might be due to the extremely large fluctuations of the terminal residues. Average interproton distances measured in model helices in ref 13 suggested that $i_\beta H_\beta \rightarrow i + 2_\beta HN$ and $i_\beta H_\beta \rightarrow i + 2_\beta H_\alpha$ may have NOE signals but were not detected by experiments. The average distances for those pairs in the current simulations are consistent with the lack of NOE in the experiment, which emphasizes that the α/β-peptide should be regarded as an ensemble of structures and it is crucial to include non-native conformations when comparing to experimental measurements.[74−76]

With the 11-helix as the starting structure, the α/β-peptide quickly deviates from the ideal 11-helix structure in both sets of explicit solvent simulations. In one set of simulations, for example, the backbone rmsd jumps to ∼5 Å after 2.5 ns (data

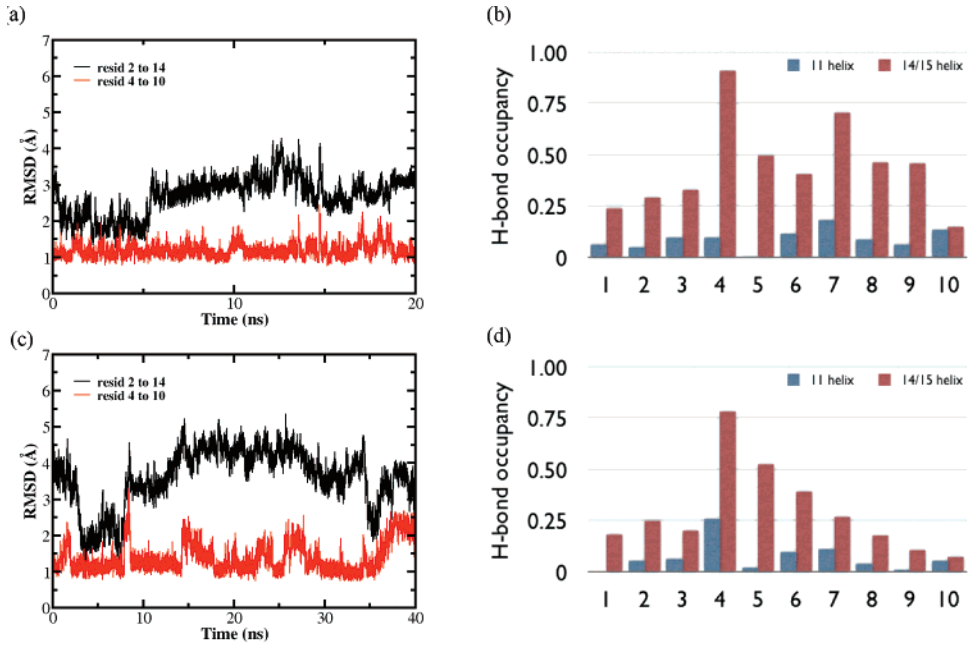

Figure 4. Results from MM simulations for a pentadeca-α/*β*-peptide with explicit solvent molecules. (a) Time dependence of rmsds in a 10 ns simulation that starts with an ideal 14/15-helix: (black line) rmsd of backbone atoms relative to the ideal 14/15-helix; (red line) rmsd of backbone atoms for residue 4−11 relative to the ideal 14/15-helix. (b) Hydrogen-bonding occupancy analysis relative to the 14/15-helical pattern. (c) Time dependence of backbone rmsds of a 10 ns simulation that starts from an ideal 11-helix: (black line) rmsd relative to an ideal 11-helix; (red line) rmsd relative to an ideal 14/15-helix. (d) Hydrogen-bonding occupancy analysis relative to the 14/15 (blue) and 11 (red) helical patterns.

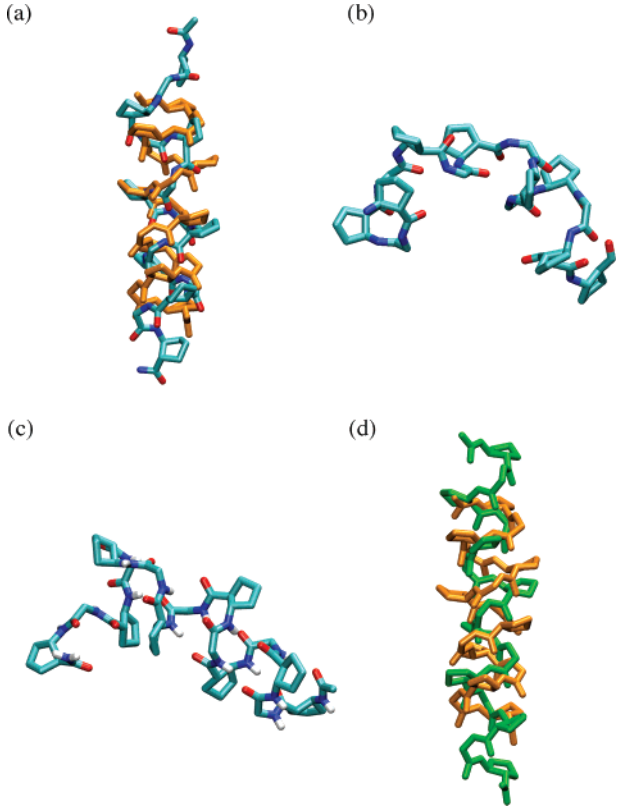

Figure 5. Representitive snapshots taken from the explicit solvent simulations of a pentadeca-α/*β*-peptide. (a) Ideal 14/15-helix (in orange) overlaid with a snapshot by the end of the simulation that starts from the ideal 14/15-helix. (b) Snapshot taken from the middle of the same simulation (rmsd ∼ 3.5 Å). (c) Snapshot of large rmsd (3.4 Å relative to the ideal 14/15-helix and 4.6 Å relative to the ideal 11-helix) taken from the simulation that starts from the ideal 11-helix. (d) Structure superpositions of ideal 14/15 (orange) and 11 (green) helices.

not shown). The structure has not completed the transition to the 14/15-helix, since the backbone rmsd with respect to the ideal 14/15-helix is also more than 4 Å for most segments of the simulations. The central part of the peptide (residues 4−10) exhibits different behaviors in two sets of simulations. In one set (Figure S6c), the rmsd relative to the ideal 14/15-helix remains in the 2−3 Å range; in the other set (Figure 4c), the rmsd is largely in the 1−2 Å range, which indicates partial conversion of the peptide to the 14/15-form (for a snapshot, see Figure 5c). Correspondingly, the backbone hydrogen bond occupancies (Figure 4d and S6d) differ for the two sets of independent simulations, although in both cases the 14/15-hydrogen-bonding occupancies are smaller than those for simulations that start with the ideal 14/15-helical form.

The fact that the α/*β*-peptide remains stable if the simulation starts from a 14/15-helix but becomes a partial 14/15-helix if it starts from an 11-helix is consistent with the PMF result that the 14/15-helix is the more stable form (Figure 3). The fact that the α/*β*-peptide does not fully convert into a 14/15-helix in the latter simulation presumably reflects the short timescale (10−40 ns) of the simulation. To better describe the distribution of α/*β*-peptide conformations, many independent and longer simulations are needed, which can be done more efficiently with an implicit solvent model.

3.2.2. Implicit Solvent (GBSW) Simulations. With the GBSW model, the significantly larger number (at least 10) and longer (∼ 20 ns) simulations (note that the timescale of an implicit solvent simulation may not be identical to that in an explicit solvent simulation,[77,78] although the value of the friction used here, 25 ps^{-1}, is quite close to the values commonly used in the literature) reveal a broad range of behaviors in terms of the conformational dynamics of the peptide, regardless of the starting configuration. Importantly, however, the results are consistent with the 14/15-helix as the more stable conformation.

With 14/15-helix as the starting conformation, the backbone rmsds for the five representative trajectories (Figure 6a) indicate that the peptide takes the 14/15-helical conformation during most of the simulation time, although substantial structural deviation (rmsd > 4 Å) is frequently observed. In some trajectories, such

TABLE 5: NOE Comparisons between Experiment and Explicit and Implicit Solvent Simulations of a Pentadeca-α/*β*-peptide[a]

NOE type	exp	solvation: explicit	solvation: implicit	NOE type	exp	solvation: explicit	solvation: implicit
$i_\beta H_\beta \rightarrow i+2_\beta HN$				$i_\alpha H_\alpha \rightarrow i+3_\beta HN$			
1 → 3	?	4.693	3.662	2 → 5	?	4.037	3.282
3 → 5	no	4.475	5.055	4 → 7	no	3.407	3.344
5 → 7	no	4.467	4.834	6 → 9	?	3.300	3.809
7 → 9	no	4.699	4.706	8 → 11	no	3.314	3.235
9 → 11	?	4.805	4.840	10 → 13	no	3.578	3.128
11 → 13	?	4.459	4.885	12 → 15	no	5.264	3.666
13 → 15	?	4.994	4.358				
$i_\beta H_\beta \rightarrow i+2_\beta H_\alpha$				$i_\alpha H_\alpha \rightarrow i+3_\beta H_\alpha$			
1 → 3	no	4.747	3.183	2 → 5	M	*3.685*	2.775
3 → 5	no	4.606	4.992	4 → 7	M	2.870	2.85
5 → 7	no	4.827	5.036	6 → 9	M	3.179	3.642
7 → 9	no	4.370	4.463	8 → 11	M	2.807	2.782
9 → 11	?	4.704	4.581	10 → 13	M	*3.558*	2.693
11 → 13	no	5.006	4.850	12 → 15	W	*4.774*	3.335
13 → 15	no	5.607	4.506				
$i_\alpha H_\alpha \rightarrow i+2_\alpha HN$				$i_\beta H_\beta \rightarrow i+4_\beta HN$			
2 → 4	?	4.840	4.322	1 → 5	W	*5.344*	*4.617*
4 → 6	No	4.475	4.374	3 → 7	No	5.466	4.562
6 → 8	No	4.554	4.889	5 → 9	No	4.381	4.655
8 → 10	No	4.385	4.331	7 → 11	No	4.381	4.437
10 → 12	No	4.472	4.343	9 → 13	?	4.298	4.398
12 → 14	No	5.107	4.557	11 → 15	?	4.843	4.259
$i_\beta H_\beta \rightarrow i+3_\alpha HN$							
1 → 4	M	*4.454*	3.473				
3 → 6	M	*4.498*	3.891				
5 → 8	W	3.574	3.786				
7 → 10	W	3.473	3.609				
9 → 12	?	3.716	3.462				
11 → 14	?	4.320	3.412				

[a] NOE distances in the simulations are calculated based on the ensemble average $\langle r^{-3}\rangle^{-1/3}$; values in italics indicate positive violations; "S" indicates a strong NOE signal (≤3.0 Å); "M" indicates a medium NOE signal (≤3.5 Å); "W" indicates a weak NOE signal (≤ 4.5 Å); "No" indicates that no NOE was observed experimentally, but the indicated NOE would have been observed if it had been present; "?" indicates that an NOE was observed, but it could not be assigned because of overlap with either a sequential or intraresidue NOE, or that more than one probable nonsequential assignment for the NOE was possible.

TABLE 6: Clusters of a Pentadeca-α/*β*-peptide from Implicit Solvent Simulations with Different Starting Configurations[a]

clusters	start with a 14/15-helix: rmsd(Å)[b]	start with a 14/15-helix: population (%)	start with an 11-helix: rmsd (Å)[b]	start with an 11-helix: population (%)
1	1.3	59.2	1.4	76.3
2	3.4	10.9	3.4	9.0
3	3.9	8.0	3.6	6.8
4	3.0	5.8	3.5	5.5
5	1.9	5.2	4.1	1.0
6	2.4	4.0	2.1	0.8
7	2.4	4.0	3.1	0.1
8	3.8	2.0		
9	3.5	0.9		

[a] For each starting configuration (either an ideal 14/15- or 11-helix), the cluster analysis is done for the combined 20 independent trajectories. See the Methods section for additional technical details. [b] Regardless of the starting configuration, the rmsd is always measured relative to an ideal 14/15-helix.

structural excursion lasts for several nanoseconds and then the structure relaxes back to the 14/15-helix (e.g., trajectories 3 and 11 in Figure 6a), while in some other cases the α/*β*-peptide remains far from the ideal 14/15-helix conformation until the end of the 20 ns simulation (e.g., trajectory 4).

To quantatively measure the 14/15-helical preference, we define helical fraction ($\lambda_{14/15}$) by

$$\lambda_{14/15} = \frac{N_{\text{frame}}(\text{rmsd} \le 2.0\text{Å})}{N_{\text{frame}}} \qquad (2)$$

where N_{frame} is the total number of frames taken from each trajectory ($N_{\text{frame}} = 200\,000$ in this work), and N_{frame}(rmsd ≤ 2.0 Å) is the number of frames with an rmsd smaller than 2.0 Å relative to the ideal 14/15-helix. As shown in Figure 6b, $\lambda_{14/15}$ is greater than 0.5 for 8 out of the 11 runs.

Results of the cluster analysis (see Table 6) further indicate that although the majority (59.2%) of the sampled configurations are close to the ideal 14/15-helical conformation, a diverse set of structures is sampled, some of which deviate as much as ∼3.9 Å from the ideal 14/15-helix with a significant population of 8.0%. In most of these conformers with large rmsds, however, the 14/15-helical structure is well maintained locally and disruption occurs only at one or two residues. For example, in the representative structure of the second most-populated cluster (Figure 7b), the ϕ of the seventh residue deviates from the ideal value and breaks the helix into two shorter 14/15-fragments. Interestingly, similar behavior is observed in the explicit solvent simulations; the structure shown in Figure 7b is very close to that in Figure 5b.

With an 11-helix as the starting conformation, all simulations converge to the 14/15-helix, although the time of conversion varies wildly ranging from several hundred picoseconds to almost 20 ns (trajectory 6) (Figure 6c). Interestingly, once converted to the 14/15-helix, the α/*β*-peptide remains rather close to that conformation, and significant deviation (>3 Å) occurs rarely beyond 1 ns. Therefore, $\lambda_{14/15}$ is in fact often larger in these simulations (Figure 6d) than for those starting with the 14/15-helix; similarly, the dominant cluster, which is very close to the ideal 14/15-helix, has a higher population (76.3% vs 59.2%) than that in the trajectories starting with the 14/15-helix. The converged 14/15-helical conformations are generally very close to those in the simulations that start from the ideal 14/15-helical structure; thus, the seemingly different stability of the 14/15-helical conformation in the two sets of simulations reflects the stochastic nature of molecular dynamics simulations. For example, similar to other explicit and implicit solvent simulations, even structures with large rmsds (Figure 7d) keep local 14/15-helical patterns. It is interesting to note that the deviation of dihedral angle ϕ from the ideal value is the cause of structural disruption in many cases, such as in Figure 7b and d (see the Supporting Information for the representative structures of other clusters).

The calculated averaged interproton distances from the implicit solvent simulations are largely consistent with those from the explicit solvent simulations and the experimental NOE pattern. In fact, the number of positive violations is decreased to one, $1_\beta H_\beta \rightarrow 5_\beta HN$, with a very small violation of ∼0.1 Å. The implicit solvent simulations tend to give shorter average distances than the explicit solvent simulations, most notably for those highlighted in Table 5.

In short, the extensive amount of sampling with implicit solvent simulations clearly shows that the 14/15-helical form is predominant for the pentadeca-α/*β*-peptide. Compared to the octamer in which the same MM model suggests that the 14/15-helical form is only marginally more stable than the 11-helix, the result here is consistent with the expectation that the wider helical form is better stabilized by dispersion interactions[79] as the length of the peptide increases,[13,14] which

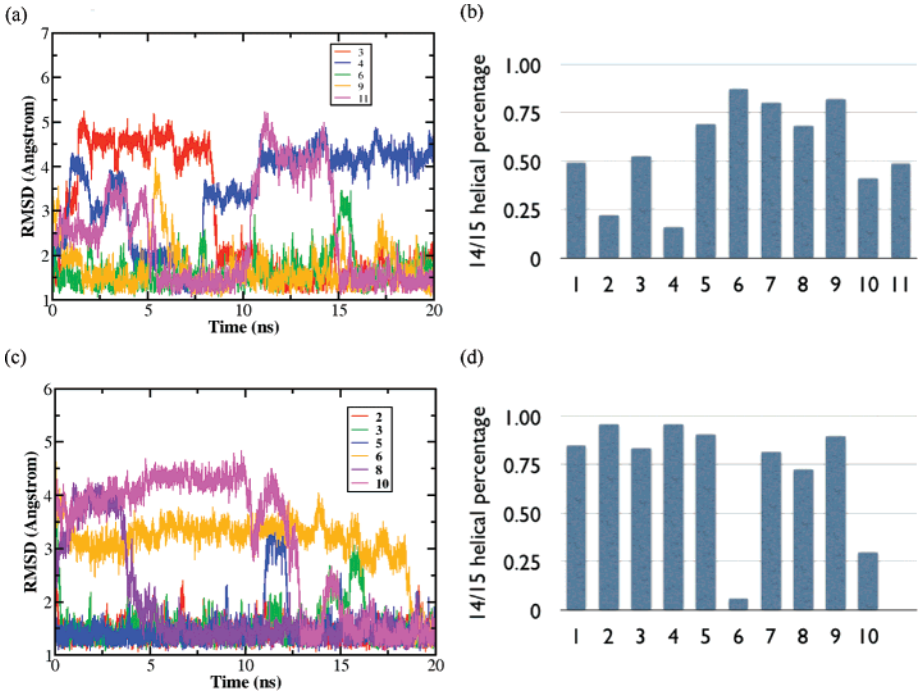

Figure 6. Results from MM simulations for a pentadeca-α/β-peptide with an implicit solvent model (GBSW). (a) Time dependence of backbone RMSDs for five randomly chosen trajectories among the 10 × 20 ns simulations that start with an ideal 14/15-helix. (b) 14/15-Helical fraction ($\lambda_{14/15}$, eq 3) in each 20 ns run that starts with an ideal 14/15-helix. (c). Time dependence of backbone rmsds for six randomly chosen trajectories among the 11 × 20 ns simulations that start with an ideal 11-helix. (d) 14/15-Helical fraction ($\lambda_{14/15}$) in each 20 ns run that starts with an ideal 11-helix.

was also observed in natural peptides.[80] Indeed, as shown in the Supporting Information, dispersion interactions appear to play a more important role than solvation in stabilizing the 14/15-helix over the 11-helix structure in the longer peptides.

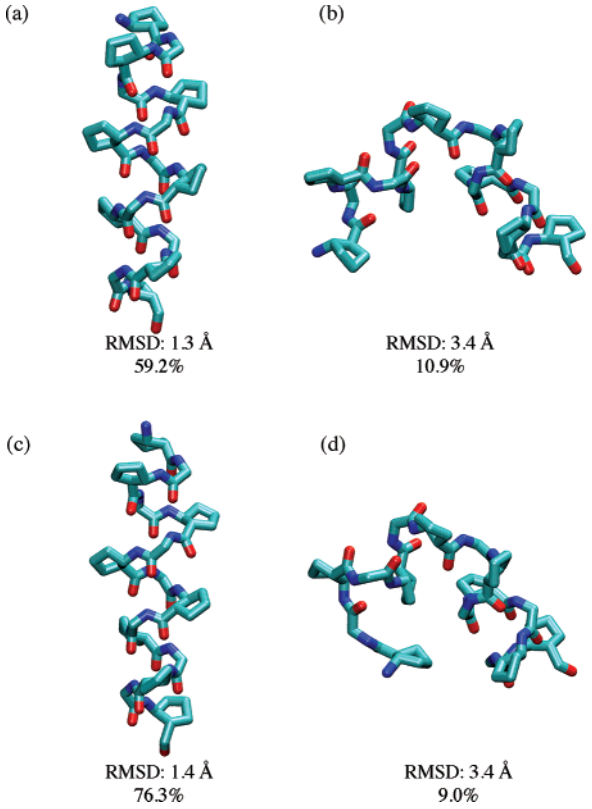

Figure 7. Representitive snapshots taken from implicit solvent simulations of a pentadeca-α/β-peptide and their populations following a cluster analysis (see the Methods section). Parts a and b are taken from simulations staring from an ideal 14/15-helix; c and d are taken from simulations starting from an ideal 11-helix. The rmsd is measured for residues 2−14 relative to the ideal 14/15-helix.

4. Concluding Remarks

We use QM/MM models to guide the development of classical models for β- and α/β-peptides. This strategy is motivated by the fact that the reliability of a QM model can be meaningfully tested in both the gas phase and condensed phase by comparing to high-level QM calculations and available experimental data, respectively.

As the first example, all-atom MM parameters for non-natural peptides with a cyclic β-residue, *trans*-2-amino-cyclopentane-carboxylic acid (ACPC), are developed using SCC-DFTB/MM simulations as the reference. The SCC-DFTB approach has been benchmarked in our recent work by comparing to high-level (B3LYP, MP2) calculations in both the gas-phase and condensed phase.[36] The MM model parametrized using a multi-objective evolutionary algorithm is found to yield both geometrical and energetic results that are consistent with SCC-DFTB/MM simulations. For example, the free energy profiles along key dihedral angles for a tetra-α/β-peptide in water are within 2 kcal/mol of those at the SCC-DFTB/MM level for regions of significant population; although there is clearly room to further improve the parametrization, this level of agreement suggests that the force field offers a meaningful starting point for studying ACPC-containing peptides using molecular simulations. In contrast, a MM model parametrized based only on frequency matching does not give satisfactory distributions, especially for the key θ degree of freedom; this difference emphasizes the importance of careful parametrization and benchmarking in developing a reliable MM model for non-natural peptides.

As the first application, the newly developed MM model is used to simulate a pentadeca-α/β-peptide with both explicit and implicit solvent (water) models. The conformational preference of the α/β-peptide in the explicit solvent simulations is sensitive

to the starting configuration, which is likely due to the limited length (~10−40 ns) of these simulations. With the implicit solvent model, much more extensive samplings are readily carried out, and the results consistently show that the 14/15-helical form is predominant for this α/β-peptide, although rather different conformations are accessible in each of the 20 ns trajectory (note that the timescale of an implicit solvent simulation may not be identical to that in an explicit solvent simulation[77,78]). The calculated NOE pattern is in close agreement with the experimental data, which emphasizes that averaging over a heterogeneous conformational ensemble is important for reproducing the experimental NOE patterns for short peptides.

With all these results taken together, it is established that effective MM models can be systematically developed for non-natural peptides such as those involving β-amino acids. The same methodology can be extended to the study of other non-natural peptide systems, which have widespread potential applications in materials science[81] and biomedicine.[2]

Acknowledgment. This work is supported by the National Science Foundation (CRC-CHE-0404704). Discussions with Dr. M. Schmitt and Mr. S. H. Choi are greatly appreciated. Q.C. also acknowledges an Alfred P. Sloan Research Fellowship. Computational resources from the National Center for Supercomputing Applications at the University of Illinois are greatly appreciated.

Supporting Information Available: Results for the MM model parametrized based on frequency-matching (AFMM). PMF results for the octamer calculated with different initial conditions are also included to evaluate the convergence of such calculations. Additional analysis of the simulation results for the pentadeca-peptide and calculations for exploring the contributions from dispersion and solvation to the stabilization of the 14/15-helix are discussed. A complete version of ref 22 is also included. This material is available free of charge via the Internet at http://pubs.acs.org.

References and Notes

(1) Cheng, R. P.; Gellman, S. H.; DeGrado, W. F. *Chem. Rev.* **2001**, *101* (10), 3219−3232.

(2) Schmitt, M. A.; Weisblum, B.; Gellman, S. H. *J. Am. Chem. Soc.* **2007**, *129*, 417−428.

(3) Appella, D. H.; Christianson, L. A.; Karle, I. L.; Powell, D. R.; Gellman, S. H. *J. Am. Chem. Soc.* **1996**, *118* (51), 13071−13072.

(4) Appella, D. H.; Christianson, L. A.; Klein, D. A.; Richards, M. R.; Powell, D. R.; Gellman, S. H. *J. Am. Chem. Soc.* **1999**, *121* (33), 7574−7581.

(5) Appella, D. H.; Christianson, L. A.; Karle, I. L.; Powell, D. R.; Gellman, S. H. *J. Am. Chem. Soc.* **1999**, *121* (26), 6206−6212.

(6) Seebach, D.; Overhand, M.; Kühnle, F. N. M.; Martinoni, B.; Oberer, L.; Hommel, U.;Widmer, H. *Helv. Chim. Acta* **1996**, *79* (4), 913−941.

(7) Seebach, D.; Ciceri, P. E.; Overhand, M.; Jaun, B.; Rigo, D.; Oberer, L.; Hommel, U.; Amstutz, R.; Widmer, H. *Helv. Chim. Acta* **1996**, *79* (8), 2043−2066.

(8) Seebach, D.; Gademann, K.; Schreiber, J. V.; Matthews, J. L.; Hintermann, T.; Jaun, B.; Oberer, L.; Hommel, U.; Widmer, H. *Helv. Chim. Acta* **1997**, *80* (7), 2033−2038.

(9) Arvidsson, P. I.; Rueping, M.; Seebach, D. *Chem. Commun.* **2001**, *7*, 649−650.

(10) Hamuro, Y.; Schneider, J. P.; DeGrado, W. F. *J. Am. Chem. Soc.* **1999**, *121* (51), 12200−12201.

(11) Cheng, R. P.; DeGrado, W. F. *J. Am. Chem. Soc.* **2001**, *123* (21), 5162−5163.

(12) Cheng, R. P.; DeGrado, W. F. *J. Am. Chem. Soc.* **2002**, *124* (39), 11564−11565.

(13) Hayen, A.; Schmitt, M. A.; Ngassa, F. N.; Thomasson, K. A.; Gellman, S. H. *Angew. Chem. Int. Ed.* **2004**, *43* (4), 505−510.

(14) Schmitt, M. A.; Choi, S. H.; Guzei, I. A.; Gellman, S. H. *J. Am. Chem. Soc.* **2005**, *127* (38), 13130−13131.

(15) Raguse, T. L.; Lai, J. R.; Gellman, S. H. *Helv. Chim. Acta* **2002**, *85* (12), 4154−4164.

(16) Hart, S. A.; Bahadoor, A. B. F.; Matthews, E. E.; Qiu, X. Y. J.; Schepartz, A. *J. Am. Chem. Soc.* **2003**, *125* (14), 4022−4023.

(17) Glättli, A.; Seebach, D.; van Gunsteren, W. F. *Helv. Chim. Acta* **2004**, *87* (10), 2487−2506.

(18) Karplus, M.; McCammon, J. A. *Nat. Struct. Mol. Biol.* **2002**, *9* (9), 646−652.

(19) van Gunsteren, W. F.; Bakowies, D.; Baron, R.; Chandrasekhar, I.; Christen, M.; Daura, X.; Gee, P.; Geerke, D. P.; Glattli, A.; Hunenberger, P. H.; Kastenholz, M. A.; Ostenbrink, C.; Schenk, M.; Trzesniak, D.; van der Vegt, N. F. A.; Yu, H. B. *Angew. Chem. Int. Ed.* **2006**, *45* (25), 4064−4092.

(20) Ponder, J. W.; Case, D. A. *Adv. Prot. Chem.* **2003**, *66*, 27.

(21) Hu, H.; Elstner, M.; Hermans, *J. Proteins: Struct., Funct. Genet.* **2003**, *50* (3), 451−463.

(22) MacKerell, A. D., Jr.; Karplus, M.; et al. *J. Phys. Chem. B* **1998**, *102* (18), 3586−3616.

(23) van Gunsteren, W. F.; Billeter, S. R.; Eising, A. A.; Hünenberger, P. H.; Krüger, P.; Mark, A. E.; Scott, W. R. P.; Tironi, I. G. *Biomolecular Simulation*: The GROMOS *Manual and User Guide*; vdf Hochschulverlag, ETH: Zürich, Switzerland, 1996.

(24) Cornell, W. D.; Cieplak, P.; Bayly, C. I.; Gould, I. R.; Merz, K. M.; Ferguson, D. M.; Spellmeyer, D. C.; Fox, T.; Caldwell, J. W.; Kollman, P. A. *J. Am. Chem. Soc.* **1995**, *117* (19), 5179−5197.

(25) Jorgensen, W. L.; Tirado-Rives, J. *J. Am. Chem. Soc.* **1988**, *110* (6), 1657−1666.

(26) Brooks, B. R.; Bruccoleri, R. E.; Olafson, B. D.; States, D. J.; Swaminathan, S.; Karplus, M. *J. Comput. Chem.* **1983**, *4* (2), 187−217.

(27) Appella, D. H.; Christianson, L. A.; Klein, D. A.; Powell, D. R.; Huang, X. L.; Barchi, J. J.; Gellman, S. H. *Nature* **1997**, *387* (6631), 381−384.

(28) Daura, X.; van Gunsteren, W. F.; Rigo, D.; Jaun, B.; Seebach, D. *Chem.—Eur. J.* **1997**, *3* (9), 1410−1417.

(29) Daura, X.; Jaun, B.; Seebach, D.; van Gunsteren, W. F.; Mark, A. E. *J. Mol. Biol.* **1998**, *280* (5), 925−932.

(30) Daura, X.; van Gunsteren, W. F.; Mark, A. E. *Proteins: Struct., Funct. Genet.* **1999**, *34* (3), 269−280.

(31) Günther, R.; Hofmann, H. J.; Kuczera, K. *J. Phys. Chem. B* **2001**, *105* (23), 5559−5567.

(32) Chandrasekhar, J.; Saunders, M.; Jorgensen, W. L. *J. Comput. Chem.* **2001**, *22* (14), 1646−1654.

(33) Glättli, A.; Daura, X.; Bindschadler, P.; Jaun, B.; Mahajan, Y. R.; Mathad, R. I.; Rueping, M.; Seebach, D.; van Gunsteren, W. F. *Chem.—Eur. J.* **2005**, *11*, 7276−7293.

(34) Kritzer, J. A.; Tirado-Rives, J.; Hart, S. A.; Lear, J. D.; Jorgensen, W. L.; Schepartz, A. *J. Am. Chem. Soc.* **2005**, *127* (1), 167−178.

(35) Rathore, N.; Gellman, S. H.; de Pablo, J. J. *Biophys. J.* **2006**, *91* (9), 3425−3435.

(36) Zhu, X.; Yethiraj, A.; Cui, Q. J. *Comp. Theor. Chem.* **2007**, *3*, 1538−1549.

(37) Field, M. J.; Bash, P. A.; Karplus, M. J. *Comput. Chem.* **1990**, *11* (6), 700−733.

(38) Gao, J. In *Reviews in Computational Chemistry VII*; Lipkowitz, K. B., Boyd, D. B., Eds.; VCH: New York, 1995.

(39) Shurki, A.; Warshel, A. *Adv. Prot. Chem.* **2003**, *66*, 249−313.

(40) Friesner, R. A.; Guallar, V. *Annu. Rev. Phys. Chem.* **2005**, *56*, 389−427.

(41) Elstner, M.; Porezag, D.; Jungnickel, G.; Elsner, J.; Haugk, M.; Frauenheim, T.; Suhai, S.; Seifert, G. *Phys. Rev. B* **1998**, *58* (11), 7260−7268.

(42) Elstner, M.; Frauenheim, T.; Suhai, S. *THEOCHEM* **2003**, *632*, 29−41.

(43) Cui, Q.; Elstner, M.; Kaxiras, E.; Frauenheim, T.; Karplus, M. *J. Phys. Chem. B* **2001**, *105* (2), 569−585.

(44) Schmitt, M. A.; Weisblum, B.; Gellman, S. H. *J. Am. Chem. Soc.* **2004**, *126* (22), 6848−6849.

(45) Vaiana, A. C.; Schulz, A.; Wolfrum, J.; Sauer, M.; Smith, J. C. *J. Comput. Chem.* **2003**, *24* (5), 632−639.

(46) Cournia, Z.; Vaiana, A. C.; Ullmann, G. M.; Smith, J. C. *Pure Appl. Chem.* **2004**, *76* (1), 189−196.

(47) Vaiana, A. C.; Cournia, Z.; Costescu, I. B.; Smith, J. C. *Comp. Phys. Commun.* **2005**, *167* (1), 34−42.

(48) Mostaghim, S.; Hoffmann, M.; Koenig, P. H.; Frauenheim, T.; Teich, J. *Proc. 2004 IEEE Congr. Evolut. Comput.* **2004**, *20−23*, 212−219.

(49) Petersson, G. A.; Bennett, A.; Tensfeldt, T. G.; Allaham, M. A.; Shirley, W. A.; Mantzaris, J. *J. Chem. Phys.* **1988**, *89* (4), 2193−2218.

(50) Frisch, M. J.; Pople, J. A.; et al. *Gaussian 03*; revision B.05., **2003**.

(51) Im, W.; Bernèche, S.; Roux, B. *J. Chem. Phys.* **2001**, *114* (7), 2924−2937.

(52) Brooks, C. L.; Karplus, M. *J. Chem. Phys*. **1983**, *79* (12), 6312−6325.
(53) Ryckaert, J. P.; Ciccotti, G.; Berendsen, H. J. C. *J. Comput. Phys*. **1977**, *23* (3), 327−341.
(54) Torrie, G. M.; Valleau, J. P. *J. Comput. Phys*. **1977**, *23* (2), 187−199.
(55) Kumar, S.; Bouzida, D.; Swendsen, R. H.; Kollman, P. A.; Rosenberg, J. M. *J. Comput. Chem*. **1992**, *13* (8), 1011−1021.
(56) Jorgensen, W. L.; Chandrasekhar, J.; Madura, J. D.; Impey, R. W.; Klein, M. L. *J. Chem. Phys*. **1983**, *79* (2), 926−935.
(57) Steinbach, P. J.; Brooks, B. R. *J. Comput. Chem*. **1994**, *15* (7), 667−683.
(58) Essmann, U.; Perera, L.; Berkowitz, M. L.; Darden, T.; Lee, H.; G., P. L. *J. Chem. Phys*. **1995**, *103* (19), 8577−8593.
(59) Nosé, S. *J. Chem. Phys*. **1984**, 81, 511−519.
(60) Hoover, W. G. *Phys. Rev. A* **1985**, *31*, 1695−1697.
(61) Anderson, H. C. *J. Chem. Phys*. **1980**, *72* (4), 2384−2393.
(62) Im, W. P.; Lee, M. S.; Brooks, C. L. *J. Comput. Chem*. **2003**, *24* (14), 1691−1702.
(63) Feig, M.; Onufriev, A.; Lee, M. S.; Im, W.; Case, D. A.; Brooks, C. L. *J. Comput. Chem*. **2004**, *25* (2), 265−284.
(64) Nina, M.; Beglov, D.; Roux, B. *J. Phys. Chem. B* **1997**, *101* (26), 5239−5248.
(65) Richards, F. M. *Annu. Rev. Biophys. Bioeng*. **1977**, *6*, 151−176.
(66) Formaneck, M. S.; Cui, Q. *J. Comput. Chem*. **2006**, *27* (16), 1923−1943.
(67) Caves, L. S. D.; Evanseck, J. D.; Karplus, M. *Prot. Sci*. **1998**, *7* (3), 649−666.
(68) Tropp, J. *J. Chem. Phys*. **1980**, *72* (11), 6035−6043.
(69) Feig, M.; Karanicolas, J.; Brooks, C. L., III. *J. Mol. Graph*. **2004**, *22*, 377−395.
(70) Mackerell, A. D.; Feig, M.; Brooks, C. L. *J. Comput. Chem*. **2004**, *25* (11), 1400−1415.
(71) Takano, M.; Yamato, T.; Higo, J.; Suyama, A.; Nagayama, K. *J. Am. Chem. Soc*. **1999**, *121* (4), 605−612.
(72) Daura, X.; Gademann, K.; Jaun, B.; Seebach, D.; van Gunsteren, W. F.; Mark, A. E. *Angew. Chem. Int. Ed*. **1999**, *38* (1−2), 236−240.
(73) Peter, C.; Daura, X.; van Gunsteren, W. F. *J. Am. Chem. Soc*. **2000**, *122* (31), 7461−7466.
(74) van Gunsteren, W. F.; Bürgi, R.; Peter, C.; Daura, X. *Angew. Chem. Int. Ed*. **2001**, *40* (2), 351−355.
(75) Trzesniak, D.; Glättli, A.; Jaun, B.; van Gunsteren, W. F. *J. Am. Chem. Soc*. **2005**, *127* (41), 14320−14329.
(76) Daura, X.; Gademann, K.; Schäfer, H.; Jaun, B.; Seebach, D.; van Gunsteren, W. F. *J. Am. Chem. Soc*. **2001**, *123* (10), 2393−2404.
(77) Snow, C. D.; Sorin, E. J.; Rhee, Y. M.; Pande, V. S. *Annu. Rev. Biophys. Biomol. Struct*. **2005**, *34*, 43−69.
(78) Feig, M. *J. Chem. Theo. Comp*. **2007**, *3*, 1734−1748.
(79) Wu, Q.; Yang, W. T. *J. Chem. Phys*. **2002**, *116* (2), 515−524.
(80) Bolin, K. A.; Millhauser, G. L. *Acc. Chem. Res*. **1999**, *32*, 1027.
(81) Pomerantz, W. C.; Abbott, N. L.; Gellman, S. H. *J. Am. Chem. Soc*. **2006**, *128* (27), 8730−8731.